
Article:
Martin, PP and Zakaria, SF (2019) Zeros of the 3-state Potts model partition function for the square lattice revisited. Journal of Statistical Mechanics: Theory and Experiment, 2019. 084003. ISSN 1742-5468

https://doi.org/10.1088/1742-5468/ab2905

Zeros of the 3-state Potts model partition function for the square lattice revisited.

Paul P. Martin*[1] and Siti Fatimah Zakaria†[1,2]

[1]Department of Pure Mathematics, University of Leeds, Leeds, LS2 9JT, United Kingdom
[2]Department of Computational and Theoretical Sciences, International Islamic University Malaysia, 25200 Kuantan, Malaysia

May 10, 2019

Abstract

We compute the exact partition function for the 3-state Potts model on square lattices of several sizes larger than previously accessible. Making comparison with the exactly solved Ising model we show that, for aspects of the analytic structure close to the ferromagnetic transition point, these lattices are large enough to approach the thermodynamic limit. Subject to certain assumptions this allows for computation of estimates for the specific heat critical exponent. We thus obtain an estimate for this exponent. The estimate is consistent with the known result, thus demonstrating the potential use of this method for other models. We also discuss the antiferromagnetic transition.

Keywords: statistical mechanics, Potts model, square lattice, universal critical exponent

This paper is dedicated to the memory of Vladimir. What PM knows of mentoring he learned from Vladimir, his mentor. Hopefully FZ will become another link in the chain.

1 Introduction

We assume familiarity with Potts models on square lattices as toy models exhibiting phase transitions — see for example [58] or [41] (and cf. e.g. Rittenberg [56] and [3, 5, 6, 21, 49]). We give formal definitions in § 1.1.

The outline of this paper is as follows. First we compute the exact partition function for the 3-state Potts model on square lattices of several sizes larger than previously accessible. Such a partition function takes the form of a huge polynomial in e^{β}. A good way to present it is to plot the zeros in the complex plane. Then the density of zeros is measured near the transition point. The specific heat critical exponent α is approximated from the zero density function. Many properties of the partition function depend heavily on system size, but this density exponent does not (for sufficiently large size). The 3-state model is not integrable, but by a trustworthy folklore the specific heat exponent is known exactly (see e.g. [5, 59]). Thus this paper obtains an approximation to a number that has been known exactly for many years! So why is it interesting?... It is interesting because the folklore gives relatively little information about the physics, and very little

*email: p.p.martin@leeds.ac.uk
†email: fatimahsfz@iium.edu.my

about the analytical 'mechanics' of phase transition modelling (cf. for example [16, 17]). The present calculation offers the prospect of an interpolation between the direct physical approaches such as in [16, 17], the renormalisation group [9, 13], and the conformal field theoretic (CFT) approach [23].

See [41, Ch.11], and references therein, for a thorough general discussion of our method. We will cite some more recent related references in § 6.

1.1 The Potts model - basic definitions

Fix a spacial dimension d. The Q-state Potts model gives representations of a bulk ferromagnet (depending on the coupling constant) in $\mathbb{R}^d$, in which spins are allowed to be oriented from Q possible spin directions. The physical spins are assumed to sit at a regular collection L of points in some interval of $\mathbb{R}^d$. This *lattice* induces a 'nearest neighbour' graph.

We take $L = \mathbb{Z}^2 \subset \mathbb{R}^2$, or some finite interval thereof; and $Q = 3$. Hence this paper studies the 3-state Potts model on the square lattice (edge directions on the corresponding graph are unimportant for us, but by convention we will consider vertical edges pointing upwards and horizontal edges pointing rightwards). It will be useful to define the model slightly more generally.

Definition 1.1. *A graph Λ is a triple $\Lambda = (V, E, f)$ where V, E are sets, and f is a function $f : E \to V \times V$.*

Fix Q a natural number and $\underline{Q} = \{1, 2, ..., Q\}$. Given a set V, a function $\sigma : V \to \underline{Q}$ is called a Q-state Potts spin configuration on V. Let Ω be the set $\hom(V, \underline{Q})$ of all spin configurations.

Definition 1.2. *For given Q the bare Potts Hamiltonian on $\Lambda = (V, E, f)$ is*

$$\mathcal{H} : \hom(V, \underline{Q}) \to \mathbb{Z}$$

given by

$$\mathcal{H}(\sigma) = \sum_{\substack{\langle i,j\rangle = f(e),\\ e \in E}} \delta_{\sigma(i),\sigma(j)}$$

where the Kronecker delta function

$$\delta_{\sigma(i),\sigma(j)} = \begin{cases} 1, & \text{if } \sigma(i) = \sigma(j) \\ 0, & \text{if } \sigma(i) \neq \sigma(j) \end{cases}.$$

Definition 1.3. *For given Q and Λ the Potts partition function is a function of a scalar β defined as*

$$Z(\beta) = \sum_{\sigma \in \hom(V, \underline{Q})} \exp(\beta \mathcal{H}(\sigma)) \tag{1}$$

We may think of $\beta = J/(k_B T)$ in which J is the coupling constant, T is temperature and k_B is Boltzmann's constant. We will not specify physical units, so here only the sign of J is significant.

Let $x = e^{\beta}$. For a given graph Λ, the partition function (1) can be written in polynomial form,

$$Z(\beta) = \sum_{\sigma \in \Omega} x^{\mathcal{H}(\sigma)}. \tag{2}$$

Roughly speaking, the partition function of a single graph is of no use and no interest — unless it is the graph Λ_{lab} corresponding to a laboratory sample of material (but such samples are so big that computing their partition function is impossible). So, what is interesting is properties of the partition function that (a) become stable through a sequence of lattices including Λ_{lab}; (b) correspond to physical observables. There are several subtleties to this statement. For brevity we refer the reader to [41, Ch.11] for these. Here we turn now to our results.

2 Raw results: zeros of partition function

We write $N \times M'$ for the square lattice with periodic boundary condition in the N direction and open boundary condition in the M direction.

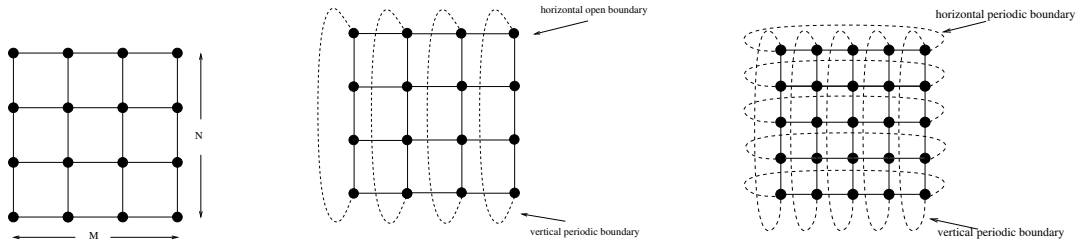

(a) (b) (c)

Figure 1: Square lattices with system size $N \times M$ and different boundary conditions.

Suppose we have 'ferromagnetic' coupling $J > 0$. Then $e^\beta \to 1$ as $T \to \infty$. If $T \to 0$ then $e^\beta \to \infty$. Thus the $x \in (1, \infty)$ region in this case corresponds to physical states.

On the other hand when $J < 0$ (antiferromagnetic coupling) then $T \to 0$ gives $e^\beta \to 0$. Here the $x \in (0, 1)$ region is the physical region.

We compute the partition function by transfer matrix methods; and zeros using a high-precision Newton-Raphson method. In terms of computation it is easier to 'grow' the $N \times M'$ lattice in the M direction than the N direction. Also finite size effects are, in practice, slightly greater with open boundary conditions, where there is a boundary. On the other hand for the analysis we will perform, making the M direction significantly longer than N makes the system into a 'thickened' 1d system rather than 2d (see [41, Ch.11] for details). A practical balance between these considerations is to have M slightly larger than N, and most of our results are for lattices of this type.

One of the biggest previous results is in [42] (see § 6 for others), with square lattice sizes up to $12 \times 13'$. These were achieved using essentially the same transfer matrix methods as results from almost twenty years earlier (see e.g. [41]), with the increase being due simply to 'Moore's Law'. Since we are interested in sequences of lattices, some of the previous results are reproduced here for comparison. Figure 2 presents the zeros distributions for square lattices with $N = 10, 11, 12$.

Almost another 20 years later, advancement of technology (again simply in the Moore's Law sense) now allows us to extend to bigger lattice sizes. Here new results are shown for $N = 13, 14, 15$. See Figures 3 to 5.

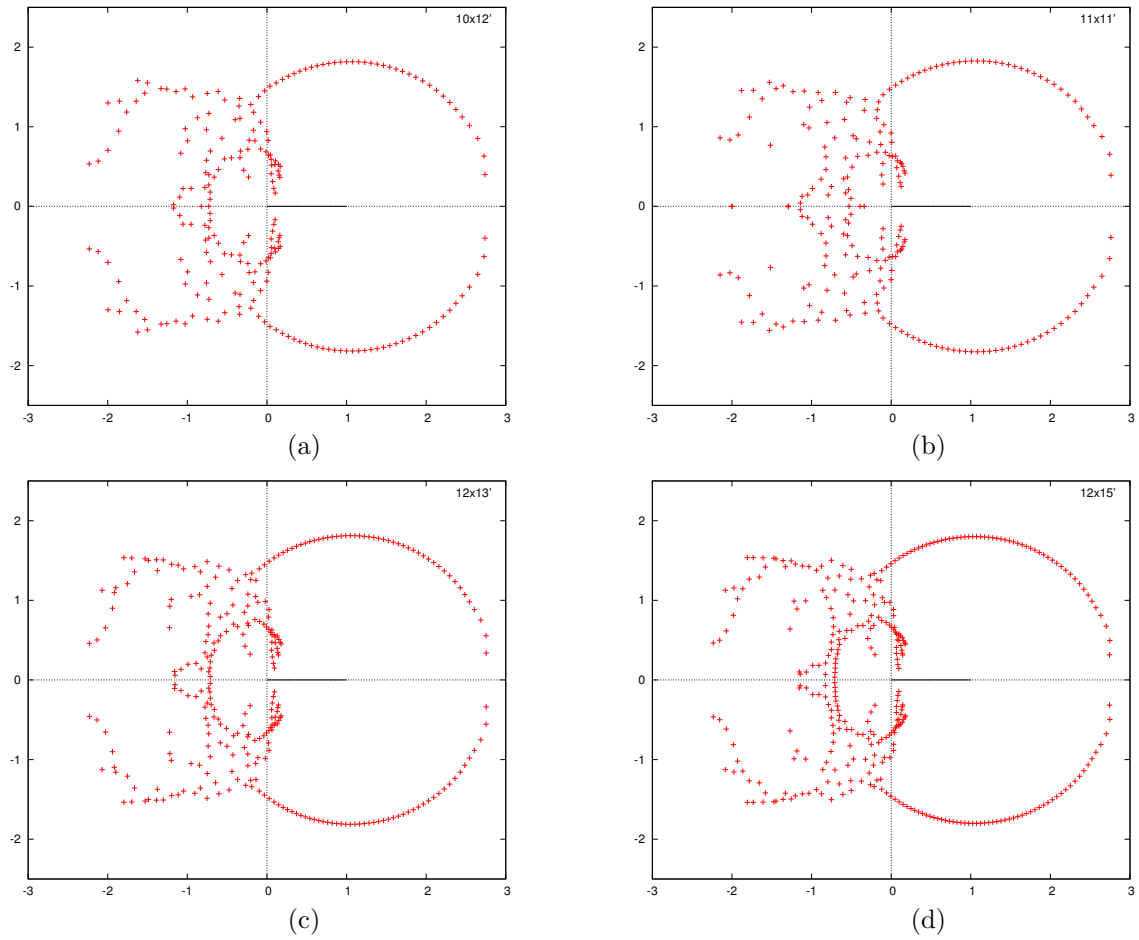

Figure 2: Zeros distribution in e^{β} for 3-state Potts models on (a) $10 \times 12'$, (b) $11 \times 11'$, (c) $12 \times 13'$, (d) $12 \times 15'$ square lattices.

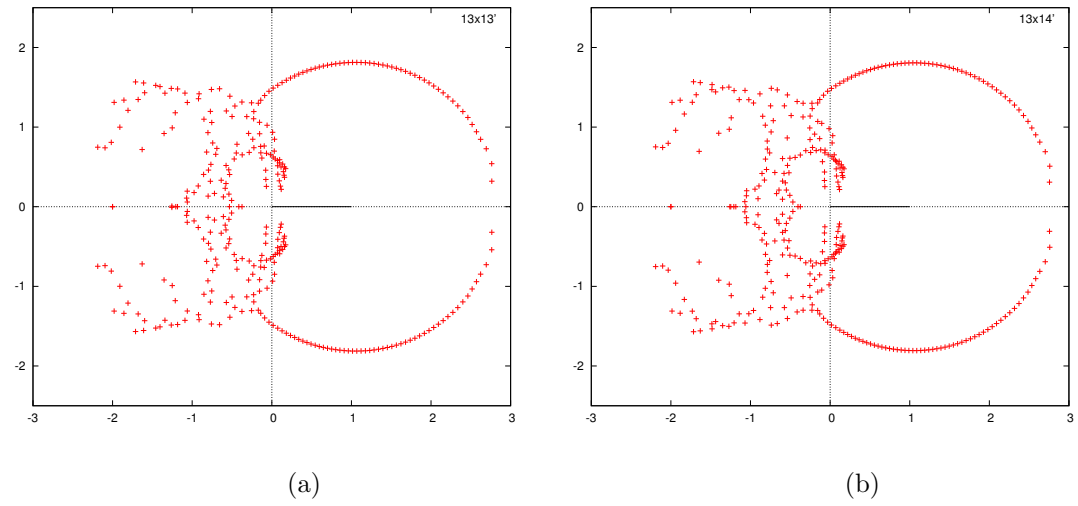

Figure 3: Zeros distribution in e^{β} for $13 \times 13'$ and $13 \times 14'$ square lattices.

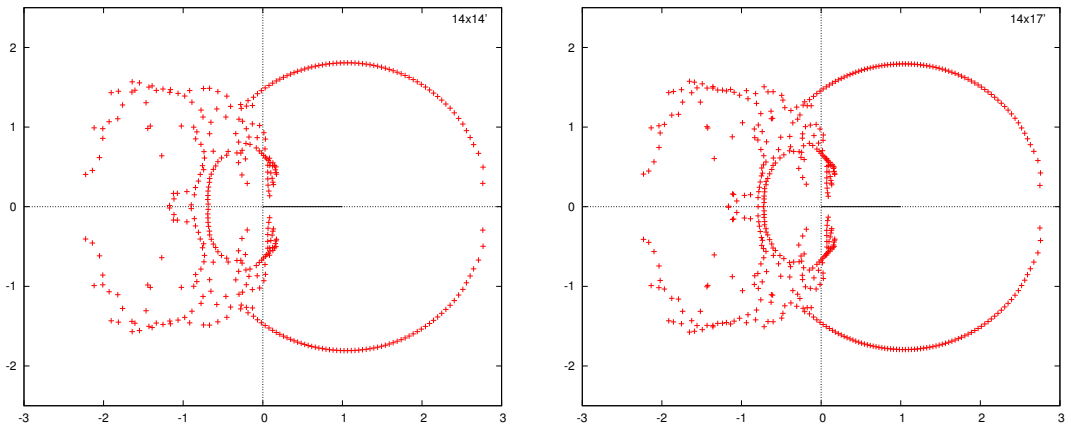

(a) (b)

Figure 4: Zeros distribution in e^{β} for $14 \times 14'$ and $14 \times 17'$ square lattices.

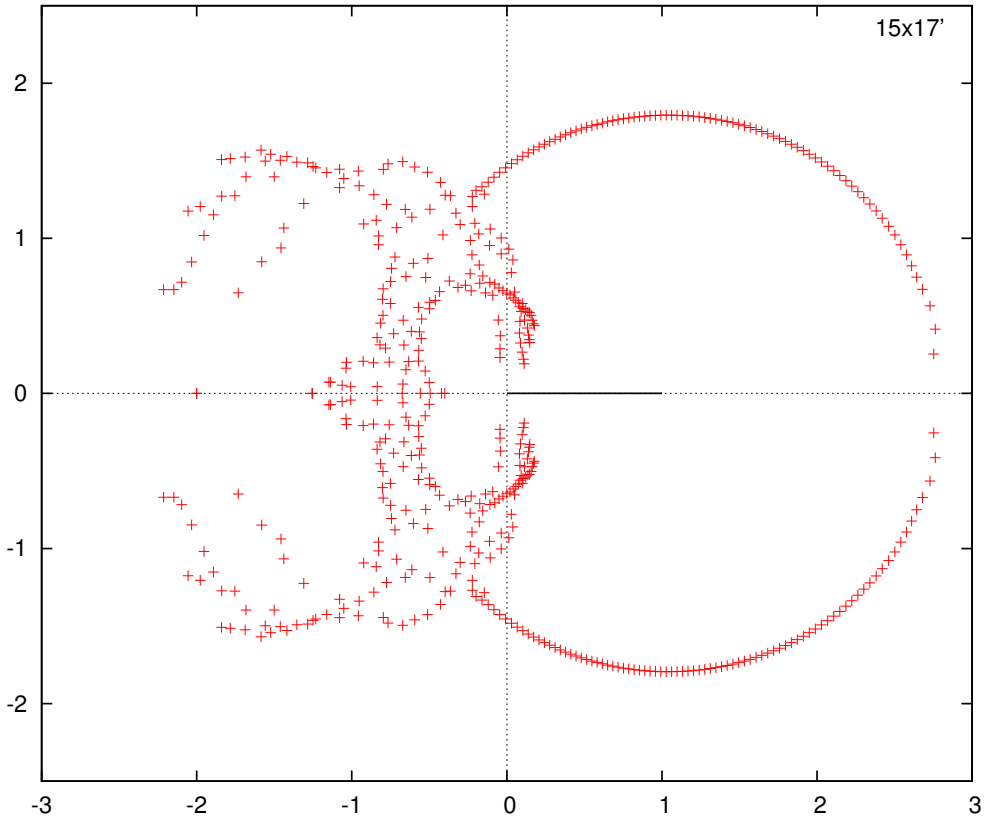

Figure 5: Zeros distribution in e^{β} for $15 \times 17'$ square lattice.

2.1 Preliminary analysis

The circular locus of zeros pinching the ferromagnetic phase transition point is in evidence as before. But two features of the distribution obfusc in earlier results have become manifest.

As we increase the lattice size, the density of zeros close to the physical region increases. The line density near the physical region can now be investigated using the new results. The line density near the phase transition is related to the specific heat universal critical exponent of the phase transition [19, 38, 41]. We will discuss this in more detail in § 3.

Second, while the complex locus in the antiferromagnetic region remains unclear, we can analyse aspects of the zeros distribution there. Baxter showed that there is a critical point of the Q-state Potts model when $(x+1)^2 = 4 - Q$ [4] (cf. also [39]). For $Q = 3$ this gives $x(x+2) = 0$, and hence a critical point at $x = 0$. Here, the zeros may form multiple lines, or become dense in some kind of 'cone'-like structure near the real axis.

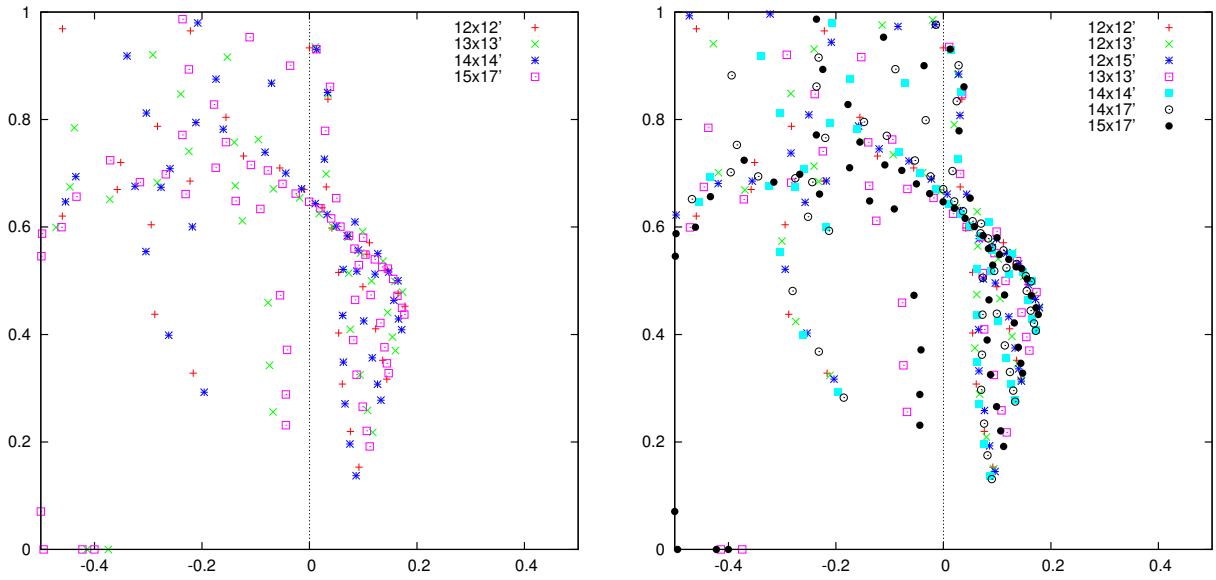

Figure 6: Accumulated zeros distributions in e^{β} close to origin for $N = 12, 13, 14, 15$.

All else being equal, we expect that the closest zeros to the physical axis occur for the largest lattice. Figure 6 shows a subtlety to this. The distribution for different lattice sizes for the $(-0.5, 0.5)$-region is shown in this figure. The closest zeros in this region are given by the square lattice of size $N = 14$, not 15. Comparing the zeros near the real axis for even and odd N suggest that the finite size effect is greater in the antiferromagnetic region than the ferromagnetic region. Such parity effects are also observed in a Bethe ansatz context in Jacobsen–Saleur [32], and are implicit in the height model treatment as for example in [12]. We shall discuss this in § 5.

2.2 Comparison with Onsager's solution: zero distributions for $Q = 2$

When addressing the question of how to analyse these results, a fresh look at Onsager's exact solution [33, 43] to the square lattice Ising model provides a useful comparison. Onsager's partition function allows us to find the zeros distribution for any square lattice (but in general for boundary conditions different from ours). (It also allows us to take the thermodynamic limit and extract critical exponents directly and exactly — which is the natural and normal approach [1]. But for

the (non-integrable) 3-state model this approach is not directly available. Instead here we will look at extracting exponents from 'stable' sequences of finite lattice cases.)

Onsager's partition function is given by [33, 43]

$$Z_{NM} \sim \prod_{k=1}^{N} \prod_{r=1}^{M} \left(\frac{(1+e^{-4\beta})^2}{e^{-2\beta}(1-e^{-4\beta})} - 2(\cos(2\pi k/N) + \cos(2\pi r/M)) \right) . \tag{3}$$

Here $\sim$ means we omit analytically unimportant overall factors, for clarity (cf. e.g. [22, 57]). This particular form requires Kaufman's boundary conditions [33]. But the aspect relevant for us does not depend heavily on boundary conditions.

For $x = e^{2\beta}$ and $C_{kr} = \cos(2\pi k/N) + \cos(2\pi r/M)$, the vanishing of each factor in (3) becomes:

$$\begin{aligned} \frac{(1+e^{-4\beta})^2}{e^{-2\beta}(1-e^{-4\beta})} - 2(\cos(2\pi k/N) + \cos(2\pi r/M)) &= 0 \\ e^{-8\beta} + 2C_{kr}e^{-6\beta} + 2e^{-4\beta} - 2C_{kr}e^{-2\beta} + 1 &= 0 \\ x^{-4} + 2C_{kr}x^{-3} + 2x^{-2} - 2C_{kr}x^{-1} + 1 &= 0 \\ x^4 - 2C_{kr}x^3 + 2x^2 + 2C_{kr}x + 1 &= 0 \,. \end{aligned} \tag{4}$$

Note that this factorises as

$$(x^2 + \alpha_+ x - 1)(x^2 + \alpha_- x - 1)$$

where $\alpha_\pm = -C \pm \sqrt{C^2-4}$. The roots of these factors are given by

$$\frac{-(-C \pm \sqrt{C^2-4}) + \sqrt{2C(C \mp \sqrt{C^2-4})}}{2} \quad \text{and} \quad \frac{-(-C \pm \sqrt{C^2-4}) - \sqrt{2C(C \mp \sqrt{C^2-4})}}{2} \tag{5}$$

It follows that the zeros lie on the locus shown in Fig.7(a), and that in the limit they become dense on this locus.

Let us put $M = N$. We are interested in the zeros close to the ferromagnetic transition point, and hence in small values of k, r, for which the quadratic Maclaurin expansion

$$C_{kr} \sim 2 - \epsilon_{kr}$$

where

$$\epsilon_{kr} = \frac{2\pi(k^2+r^2)}{N^2}$$

is good. We have

$$C^2 - 4 = (C+2)(C-2) \sim -4\epsilon_{kr}$$

Substituting in (5) (first case) we get

$$\frac{2 \mp 2i\sqrt{\epsilon_{kr}} \; + \; 2\sqrt{2}(1 \mp i\sqrt{\epsilon_{kr}})}{2} \quad \rightsquigarrow \quad (1+\sqrt{2})(1 \mp i\sqrt{\epsilon_{kr}})$$

close to the critical point at $x = 1+\sqrt{2}$. From this we see that the imaginary part is

$$\sim \sqrt{\epsilon_{kr}}$$

while the real part varies much more slowly with k, r. (N.B. This simple analysis was well-known from Onsager's result. But we now use it to test a computation for the exponent which generalises to other models.)

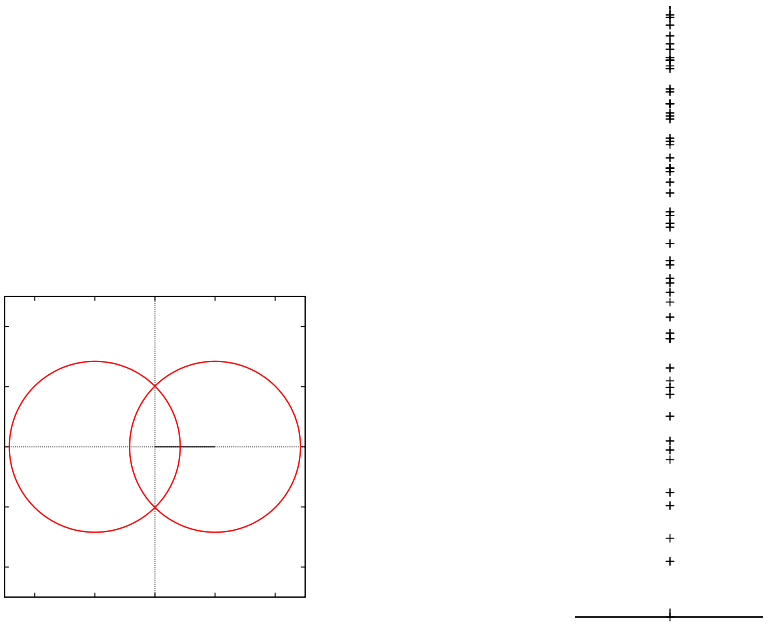

Figure 7: Square lattice Ising model (a) Locus of zeros in x (scale is given by unit length of solid segment of positive real axis); (b) blow-up of zeros close to critical point.

As we will see below, we wish to determine the large-N-asymptotic position dependence of the density of points on the line close to 0 given by the set $\sqrt{\epsilon_{kr}}$ as k, r vary. Note from our analysis that the zeros lie on the loci shown in Fig.7(a); and, for sufficiently large lattice, the blow up of the part of the first quadrant very close to the phase transition point is given by Fig.7(b).

Note that this zero distribution is the same up to an overall scale for every sufficiently large lattice. The scale does not affect the exponent (see below), so in this sense this figure gives the thermodynamic limit *even though it is discrete*.

Caveat: Kaufman's boundary conditions are not physical. For physical boundary conditions there cannot be a zero on the positive real axis. However the differences in boundary conditions become irrelevent in the thermodynamic limit, so for us they are simply part of the finite-size effects that we must control in our analysis below.

It might also be interesting to compare with the cubic lattice Ising model. This is not integrable, but see for example [8, 38, 44, 54].

3 Zero density analysis I: theory and benchmarking

In our results above we observe the tendency of the *locus* of zeros to stabilise for larger lattices. This is well-known (if not fully understood). But our progress with computing bigger lattices gives us the opportunity to begin a more sophisticated and useful analysis of the zeros distribution.

Formally the locus of zeros determines the phase transition points, which could be considered physical. But these are not universal properties, and so are not in practice experimentally quantitatively observable. The most natural observable properties to consider are critical exponents.

The general theory connecting density of zeros to the specific heat critical exponent is given for example in [41, §11.1].

In short, the setup is as follows [38, 39, 41]. Let y denote the distance away from the critical

point in the complex plane (note that, for differences, working with x or β is asymptotically the same). Suppose the density of zeros $a(y)$ obeys a power law for small y, that is

$$a(y) \sim |y|^{1-p}. \tag{6}$$

for $0 \leq p < 1$. The specific heat is then given by [41]

$$\frac{dU}{d\beta} \overset{(\beta-\beta_c)\to 0}{\sim} |\beta - \beta_c|^{-p}.$$

This gives the critical exponent $\alpha = p$.

3.1 On zero density in the discrete case

A laboratory sample of a ferromagnet is, of course, not infinite. The physicist's interest in the thermodynamic limit stems from the assumption that laboratory samples are large enough that suitable intensive observables have stopped depending on system size — so that the infinite lattice result is as good as the one we want, the large finite lattice result. So in the present context the question arises: what does the zero density analysis above look like for a finite system that is big enough to be in the limit?

The natural answer is that if we break the complex neighbourhood of the transition point up into several very small finite equal intervals ('bins') and count zeros in the intervals then the variation as we move away a short distance from the critical point along the line (i.e. in some non-real direction in the complex plane) will discretely reflect the limit dependence. In the *power law* cases of interest this implies that a log-log plot of frequency in a bin against distance from the critical point will (for sufficiently large systems) have a constant gradient; we will get the same gradient for all sufficiently large systems; and the gradient is $m = 1 - \alpha$.

Observe that several conditions must be in place for this to work. In order to have a verifiable constant gradient we need several bins. And to have several bins close to the transition point the bins must be small. But in order for the number of points in a small bin to *not* be small (else we will have discretisation errors) the number of points must be high. So the system must be large. None of these observations gives us quantitative estimates of the size needed. Practical verification must then arise from finding bin sizes that give a constant gradient to high accuracy; and from confirming that this constant is stable with (sufficiently large) system size. (Remark: It seems likely that a system satisfying the former condition will necessarily satisfy the latter. But we will test both.)

Here the data for the log-log graph is obtained as follows. A working assumption is that, sufficiently close to the critical point, the zeros in x lie on a line essentially perpedicular to the real axis. Note from the results above that this is valid in our case (but cf. § 5). In this case the distance y from the critical point can be taken to be given by the imaginary part, and bins constructed accordingly. However for a lattice of finite size there will not be many zeros 'arbitrarily' close to the critical point, in which case the larger scale structure of the locus is relevant to how y is measured. Here the first quadrant in the complex plane is divided into several segments of equal angle from the centre of the circular locus. This is somewhat ad hoc (cf. for example the analysis discussed in [41, §11.1]), but any procedure which constructs essentially similar bins close to β_c is equivalent in the limit. We number the bins $1, 2, ..., b$ from the real axis. The total number of zeros in each bin Δ_i is then counted and plotted against the mid-point value of y in Δ_i, in the log-log plot. We use only the bins closest to the real axis — which we take to be those up to the high point of the circular locus.

Linear regression line fitting is used to fit the log-log plot, and to give a quantitative measure of the quality of linear fit. For various reasons the linear fitting is predicted to work near the transition point (first few bins), and not necessarily further away. But as noted, we do not have a quantitative guide for what 'near' means, so we run the fit until it fails.

3.2 Benchmarking with the Ising model

Here we examine the zeros from Onsager's partition function. For 100×100 square lattice (and others), the log-log plot gives a line distribution as illustrated below. Changing the number of bins (within a range that keeps down discretisation effects) does not greatly affect the log-log graph. The gradient is approximately $m \sim 1$ which gives $\alpha \sim 0$. This observation supports the method, since we know that $\alpha = 0$ for the Ising model (see e.g. [1, 59]).

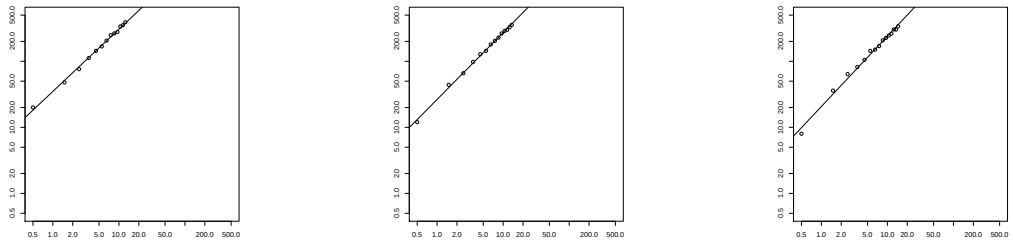

(a) Number of bins, $b = 13$. (b) Number of bins, $b = 14$. (c) Number of bins, $b = 15$.

Figure 8: Lattice size 100×100, $Q = 2$: Bin occupancy and linear regression analysis.

Fig.9 is the version for a large lattice ($N \geq\sim 1000$) in the asymptotic region using our analysis above. It is interesting to note (for reference below) that the first bin is (very slightly) an outlier, even in the limit.

The very simple but rather beautiful distribution in Fig.7(b) has been discussed many times, in a variety of contexts. See for example [1, 20]. We reiterate that it is of interest to us now for comparison to the $Q = 3$ result. In particular note the irregularity of the pattern on the small scale (which would here defeat a simple analysis of the type proposed in [41, p.294] for example). The $Q = 3$ result, even for much smaller lattices, is much more regular in comparison. The ferromagnetic loci look superficially similar between $Q = 2$ and 3 because of the large scale geometry, but this shows that they are substantively different. We will develop this point in a separate work.

4 Zero density analysis II: 3-state Potts model

Here we apply the analysis from § 3.1 to the 3-state Potts model zeros distributions. Our first examples use bins radial from the centre of the ferromagnetic circular locus, from the axis to vertical. Firstly for $15 \times 17'$ with number of bins $b = 10, 11, 12$. Note that the first bin can be empty, in which case we omit it — this is ad hoc, but there are plenty of bins:

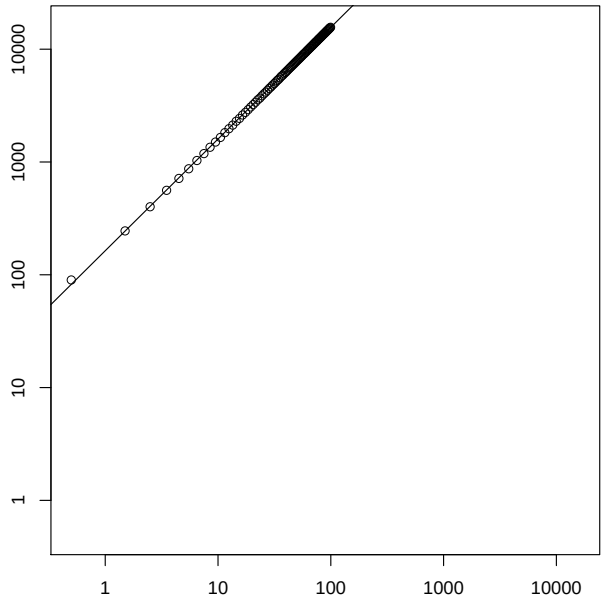

Figure 9: Scaled asymptotic bin occupancy for $Q = 2$, $b = 100$.

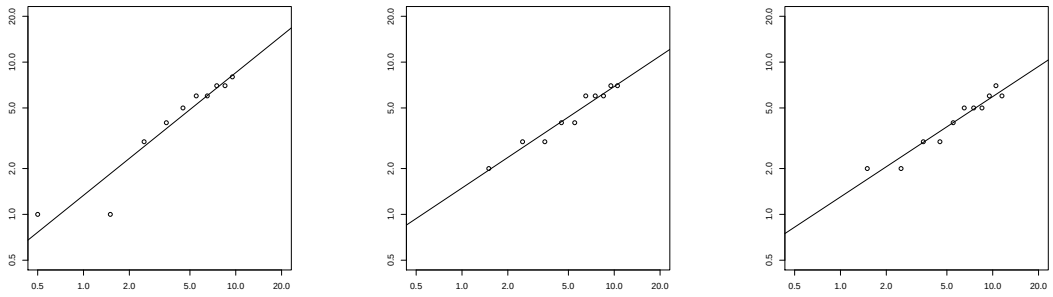

The linear regression fits to these give slope $m = .8, .67, .66$ with standard deviations $.09, .05, .06$ respectively. (Recall that the exact value is $2/3$, giving $\alpha = 1/3$.) Fig.10 gives $N = 14$.

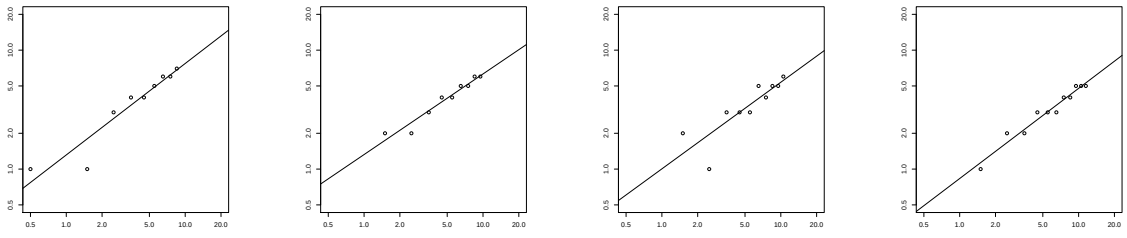

Figure 10: Case $N = 14$, $b = 9 - 12$. Linear fit $m = .77 \pm .1,\ .68 \pm .06,\ .73 \pm .16,\ .76 \pm .05$.

Another way to extract a density from the discrete data, in principle, is to plot the separation of

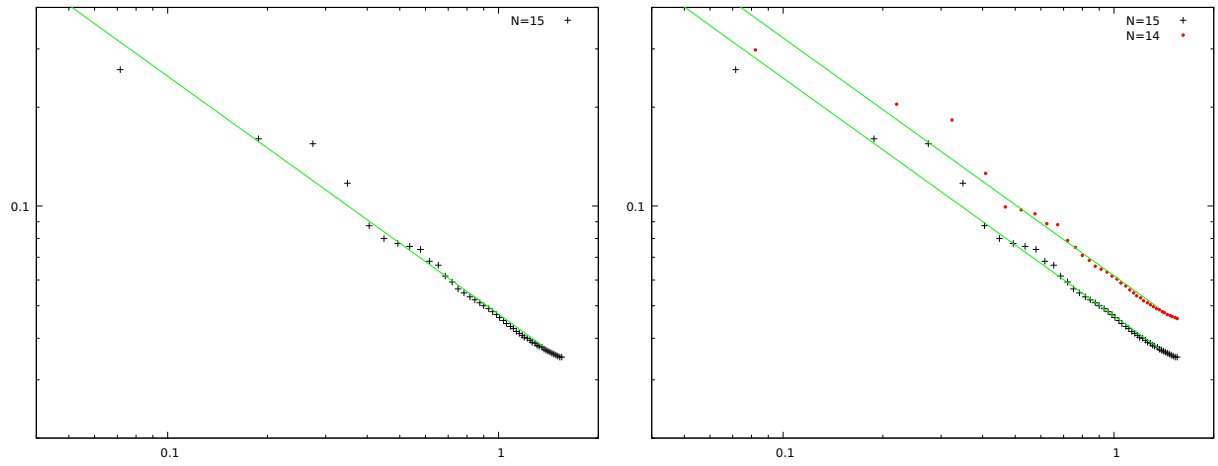

Figure 11: Separation versus locus distance from critical point for $15 \times 17'$ and $14 \times 14'$.

zeros against distance from the critical point. Under suitable circumstances separation is inversely proportional to density. This would not work in the $Q = 2$ case since there is too much fine structure in the distribution. The log-log plot here is in Fig.11. The gradient (with opposite sign due to the inverse) is $.72 \pm .02$. The regression fitted gradient is the same for $N = 15$ and 14, and indeed even the pattern of zeros looks similar, much as happens for the thermodynamic limit Ising model above (although the pattern is intriguingly different between the two models). However the gradient is slightly too high, so there is something very interesting to investigate further here.

To test for finite-lattice sensitivity to the method of division into bins see Figs.12 and 13; and Table 1. These give results using bins radial from the *origin* (b is the number of bins in the positive quadrant, but again we keep only bins meeting the ferromagnetic locus before the high-point of the circle). Several further variants on these plots can be found in [60].

(a) Number of bins, $b = 9$.

(b) Number of bins, $b = 10$.

Figure 12: Lattice size $14 \times 14'$: Linear regression on log-log plots.

Discussion. We use linear regression to get objective numerical estimates, but even supported by visual checks (the 'Manual' column is obtained by eye with a ruler) linear regression on log-log plots is a famously tricky way to extract exponents and error bars (there are analogous problems even with experimental data). So there is no claim that the above is a complete engine for computing exponents. Bluntly put, the combined analysis above gives something like $\alpha \sim .3 \pm .1$. But what is

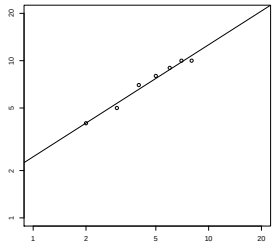

(a) Number of bins, $b = 11$.

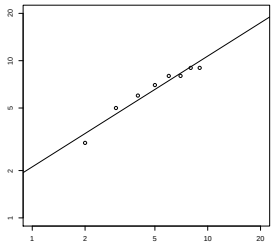

(b) Number of bins, $b = 12$.

Figure 13: Lattice size $15 \times 17'$: Linear regression on log-log plots.

Table 1: Fitted slope m of log-log plot for $14 \times 14'$ and $15 \times 17'$ square lattices.

Lattice size	$14 \times 14'$			$15 \times 17'$		
Bin, n	Lin. reg.	Std. dev.	Manual	Lin. reg.	Std. dev.	Manual
6	0.5858	0.1611	0.75	0.4933	0.11493	0.6
7	0.7688	0.09357	0.6	0.5344	0.13894	0.8
8	0.69276	0.11134	0.7	0.6109	0.08523	0.7
9	0.67331	0.08984	0.6	0.7027	0.08235	0.6
10	0.74003	0.09145	0.7	0.7116	0.10301	1
11				0.7128	0.04786	0.7
12				0.7047	0.06792	0.7

interesting is that the numerics are close enough that we can indeed study quantitatively the *way* the analytics manifests the phase transition.

5 On the antiferromagnetic region

For various reasons, such as the complexity of the ground-state, we expect that finite size effects are more severe in the antiferromagnetic region. And in any case it will be evident from the main figures that the locus of zeros is more complex than the ferromagnetic locus. Nonetheless, we can make some interesting observations from our results. Recall Baxter's formula for the critical AF Q-state Potts model [4] is $(x+1)^2 = 4 - Q$, which at $Q = 3$ gives $x(x+2) = 0$ (see also [39]). This says that the antiferromagnetic critical point is at temperature $T = 0$, which corresponds to the origin in the complex x plane. We now focus briefly on the zero distribution in the neighbourhood of the antiferromagnetic region — the antiferromagnetic region is the interval $(0, 1)$ of the real line in the complex x plane. See Figure 6 for the zeros distribution for the antiferromagnetic neighbourhood, for $N = 12, .., 15$.

In the ferromagnetic region, as the lattice size is increased the closest zeros approach the real axis monotonically. The zeros in the antiferromagnetic region converge to the axis less straightforwardly with system size. However consider the separate even and odd N plots in Figure 14. Each individual sequence in this figure is 'moving closer to' the real axis as the size increases.

In the Ising model, the antiferromagnetic groundstate is frustrated on small periodic lattices for odd N, and this indeed leads to a parity-dependent size effect. However this kind of alternating groundstate is only one of many for $Q = 3$, and there are other patterns that are frustrated by even N (cf. e.g. Burton–Henley [10], Cardy *et al* [12]), so it is intriguing that there is a noticable odd/even dependence in our data. (Confer also Jacobsen–Saleur [32] and references therein.)

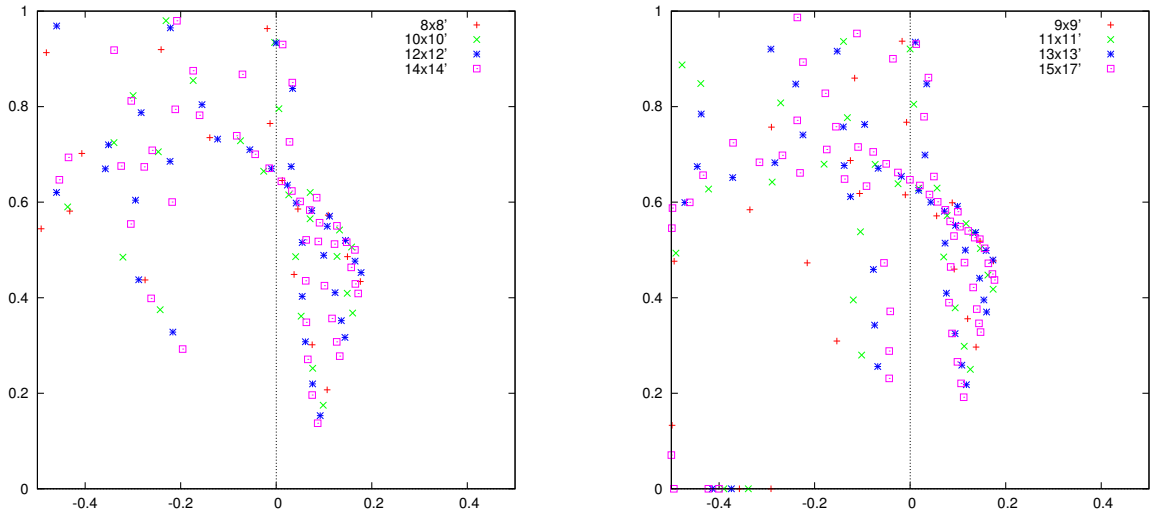

(a) (b)

Figure 14: Antiferromagnetic region in e^{β} for lattice sizes with a) even N and b) odd N.

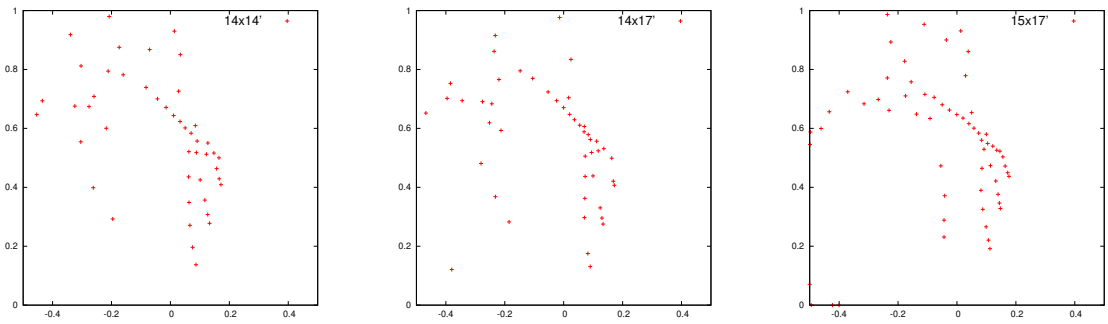

Figure 15: Antiferromagnetic region. Individual cases.

The present data seems unlikely to yield an accurate specific heat exponent. But we can investigate the 'fine structure' in the size dependence.

Observe that in all computed cases there is, for each of the two critical points, a unique complex conjugate pair of zeros closest to it (see e.g. Fig.15). Let the distance from closest zero to critical point be denoted d_f and d_{af} respectively. To separate out the odd/even effect from the size effect, consider the ratio. See Table 2. Note the marked parity dependence. Can we explain this?

Table 2: Closest zeros distance from critical points and their ratio for different N.

N	d_f	d_{af}	$r = d_{af}/d_f$
10	0.436885	0.200684	0.4593520034
11	0.391279	0.280068	0.7157756997
12	0.353739	0.178626	0.5049655254
13	0.322341	0.247607	0.7681523604
14	0.295721	0.162422	0.5492406694
15	0.255333	0.222039	0.8696055739

Write the partition function in the form

$$Z = \sum_{i=0}^{2NM-N} a_i x^i.$$

Thus a_0 is the degeneracy of the antiferromagnetic groundstate. Does this have a significant parity dependence? For a 3-state Potts model on a *one-dimensional* N-site lattice with periodic boundary condition — a ring, the antiferromagnetic ground states are the 'Barlow sequences' (see e.g. [53]), so the degeneracy is given by the Barlow number [51]:

$$b_N = 2^N + 2(-1)^N \text{ for } N > 0. \tag{7}$$

Every ring groundstate induces 2d groundstates in an obvious way (start with the ring as a first layer and add further layers each by applying $+1$ or -1 (mod.3) to the whole ring configuration).

So let us compare the number of antiferromagnetic ground states between the one-dimensional case and the $N \times M'$ lattice case.

We normalise the groundstate multiplicities by expressing them as a fraction of *all* configurations. We make intensive quantities by taking the appropriate root of the ratio. Obviously $\sqrt[N]{b_N/3^N}$ converges rapidly to 2/3. The odd/even difference is essentially undetectable from about $N = 7$. Table 3 tabulates this with

$$r_M = \sqrt[M]{\frac{a_0}{3^{NM}}} \tag{8}$$

and

$$r_{NM} = \sqrt[N]{r_M}. \tag{9}$$

The asymptotic value of r_{NM} for large N, M is known. This is via Lenard's observation of the equivalence with the ice model solved by Lieb in [35, 36] (see also [2] and [5, §8.13]). The asymptotic value is $\frac{1}{3}(\frac{4}{3})^{2/3} \sim .5132$.

Fig.16 shows that the odd/even difference persists for much longer in 2d. This might explain the noted parity difference in the zero distributions, but raises its own questions. The even sequence appears to be converging monotonically to the asymptotic value, but the odd sequence does not. Jacobsen–Saleur give a technical explanation for the odd-even difference in [32], but further number-theoretic fine structure within the convergence of the odd sequence is not ruled out there. We will further address these challenges elsewhere.

Table 3: Antiferromagnetic groundstate ratios and roots (here $M = N$ except for $15 \times 17'$).

N	$\sqrt[N]{\frac{b_N}{3^N}}$	a_0	$\frac{a_0}{3^{NM}}$	r_M	r_{NM}
3	0.6057	24	0.00121933	0.1068334089	0.4744994304
4	0.6865	4626	0.000107465	0.1018161711	0.5648773878
5	0.6581	38880	4.59E-008	0.0340674062	0.5087071172
6	0.6700	37284186	2.48E-010	0.0250722546	0.5410020343
7	0.6651	1886476032	7.88E-015	0.0096659433	0.5154395618
8	0.6673	9527634436194	2.77E-018	0.0063885629	0.5317106966
9	0.6663	2825260002442752	6.37E-024	0.0026466285	0.5171690832
10	0.6667	77048019386429374638	1.49E-028	0.0016499225	0.526922027
11	0.6666	132046297983569105731584	2.45E-035	0.000713757	0.5175581207
12	0.6666	196988209730968720777073734 50	3.88E-041	0.0004289582	0.524044193
13	0.6666	193554351965524736352758387687424	4.50E-049	0.0001909958	0.517517353
14	0.6666	159147870862104841838351532192943853490	4.85E-056	0.0001119444	0.5221387133
15	0.6666	29274766481378105714861373681423215500710370349 96	6.32E-074	0.0000494483	0.516349101

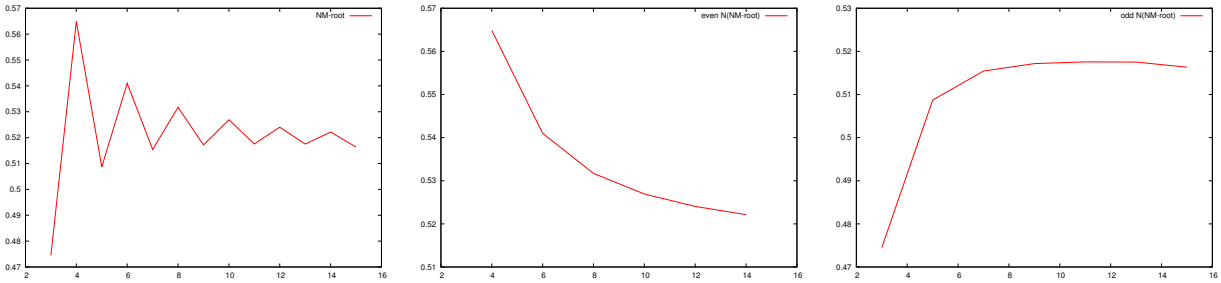

Figure 16: The NM^{th}-roots for (a) all N; (b) even N; (c) odd N.

5.1 Comparison with other models

For context it might be helpful to recall aspects of what is known of the AF region by other methods. As noted, regarding Q as a variable the AF critical curve corresponds to an integrable model, through the work of Baxter [4], so our zero-temperature point is the point $Q = 3$ there. The phase diagram and results from conformal field theory were discussed in beautiful work of Saleur [48]. A detailed investigation of the AF critical theory was initiated by Jacobsen and Saleur [32]. See also [12, 24–28] and [11].

In [12] Cardy *et al* use a height model realisation to study the AF critical point. This reveals a role both for a relevant scaling operator and a marginal one. This recalls other models such as the XY model (see e.g. [5]) and in particular the 6-state clock model (see e.g. [16, 17, 41]). To give a framework for discussing the various models from our perspective we use the χ-model notation for $\mathbb{Z}_Q$-symmetric models discussed for example in [41, §11.4]. Thus $\chi = (\chi_0, \chi_1, ..., \chi_{Q/2})$ means that the Hamiltonian contribution at a lattice edge where the two spins differ by i is given by χ_i (so in particular if χ_0 is largest then the naive ferromagnetic groundstate is ordered). For example $\chi = (1, 0, 0, ...)$ is the Potts model.

For comparison we reproduce here zero distributions for the 6-state clock model in the form of the $\chi = (3, 2, 1, 0)$ model; and the 5-state $(3, 2, 0)$ model. As discussed in [41] the ferromagnetic $(3, 2, 1, 0)$ model is a possible candidate for a three-phase model with continuous variation in the middle phase; while the $(3, 2, 0)$ model might simply have two stages of order-disorder transition.

See Figure 17. Here one is focussing on the ferromagnetic region, and so on the band of zeros approaching the marked part of the positive real axis (note these figures are plotted in $e^{-\beta}$); while the comparison is with the zeros approaching the AF critical point in our 3-state model figures. (For lattice of different sizes, and for more such phenomena in the 6-state setting, confer for example [41] and [60].) Of course present lattice sizes are too small to draw conclusions from these comparisons, but they are certainly intriguing.

Noting that the height model can be considered as a restricted 6-state model, it would of course be interesting to interpolate between the various models under consideration. A naive way to do this is to consider the $\chi = (0, A, 0, B)$ 6-state models for large $A > B$. At low temperature for very large A, B this Hamiltonian forces a parity change between the odd and even sublattices. Thus firstly in the groundstate (having fixed the parity of a single site) only three states are possible on each sublattice. Using the height model shift (see e.g. [12, §2]) this becomes a 3-state model, and the groundstate coincides (up to fixing) with that of our AF 3-state model (after the shift, the B energy level corresponds to adjacent sites having the same spin). Unfortunately for our purposes the energy-entropy trade for finite A, B is such that the phase structure is dominated by the full 6-state model. But the approach is intriguing and we include the zero distributions for a sample of A values, with $B = A - 1$, for the reader to ponder — Figure 18. We will return to this in a separate work.

6 Discussion

We conclude by discussing comparisons between this work and various beautiful existing studies not already mentioned. (We thank the referees of the article for encouraging this.)

On boundary conditions — self-dual, periodic and so on. An early point of interest in this topic, in the 1980s, was the shape of the locus of zeros in the neighbourhood of the ferromagnetic transition. Since there is only one ferromagnetic phase transition point this point must be fixed under duality, which thus determines it. If one supposes that the locus of complex zeros is a simple line meeting the real line in this one point, then duality has to coincide with complex conjugation on this locus, and the locus is also determined. (Note that the simple line property is only known to be true in a neighbourhood of the transition point [21], and indeed it is not true in general.) The real-point argument can be found in many places, see e.g. [2, 4, 5, 58], and the complex locus argument can be found for example in [39, 41]. Thus from the outset it was of interest to consider zeros for lattices exactly preserving self-duality. Such results can be found in [39–41] (see in particular Fig.11.1 in [41]), and this variant of the problem is also explored for example in [15] and [34]. All these results evidence clearly that the locus of zeros is indeed the 'duality circle' in a significant complex neighbourhood of the transition point. But of course as already noted the shape of this locus itself is not physical. We computed updated results for self-dual boundary conditions (see e.g. [60]), but they do not of themselves shed any new light on the problem. The breaking of exact self-duality is essentially a finite-size effect not radically different, in physics terms, to the other finite-size effects operative here.

On computation — Newton-Raphson and so on. Finding the zeros of a large polynomial is an intrinsically interesting problem in computer science. In general the most effective algorithm can even depend on properties of the class of polynomials under consideration. In our case we have no problem to compute all the zeros by only mildly sophisticated variants of Newton–Raphson. Since we focus on the physics rather than the computation in this paper, we do not dwell on this point here. (Another important technical tool for us is the Gnu multiple-precision library.)

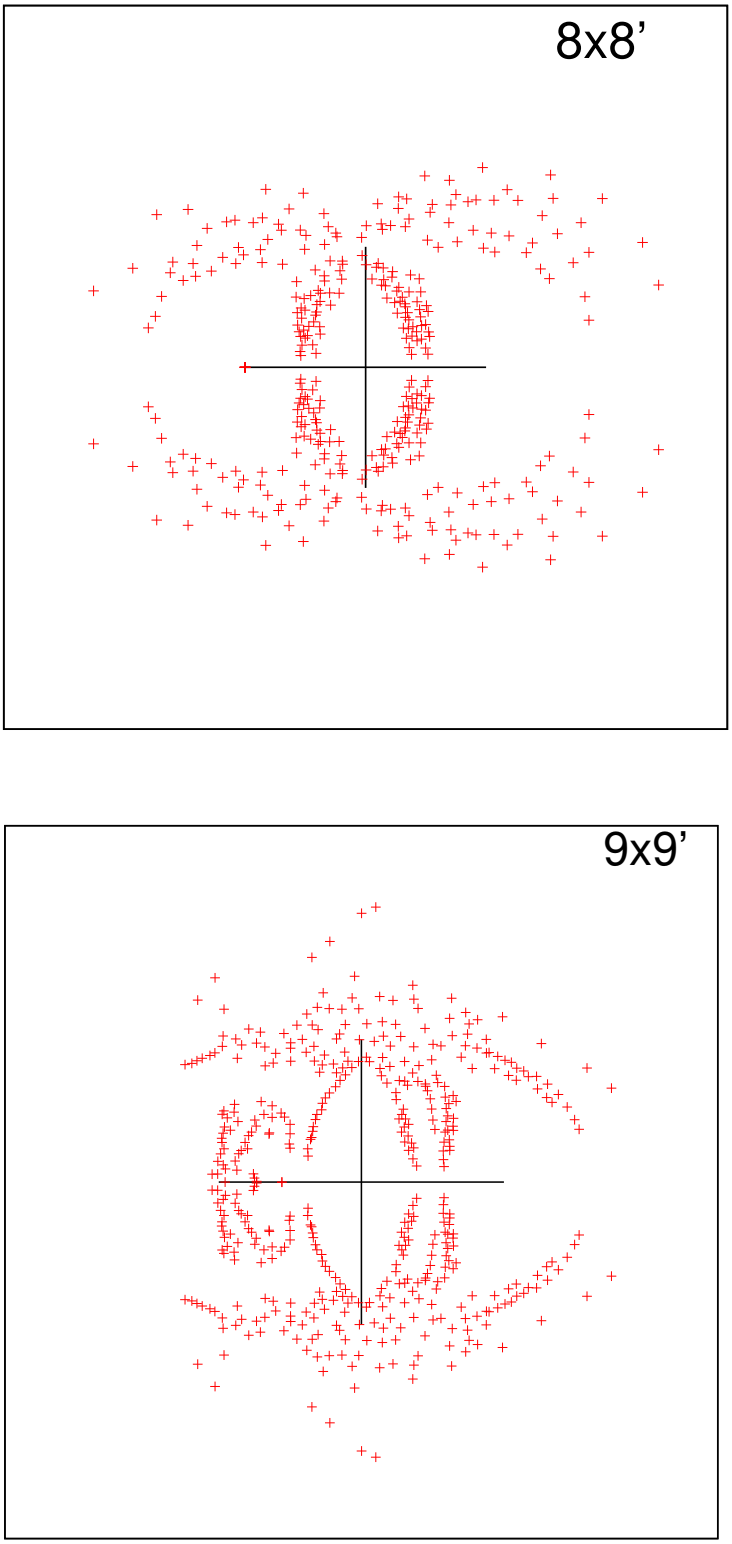

Figure 17: Zeros in $e^{-\beta}$ for the $\chi = (3, 2, 1, 0)$ 6-state model (above) and $\chi = (3, 2, 0)$ 5-state model (below) with lattice sizes as shown. The scale is set by unit length of the positive real axis.

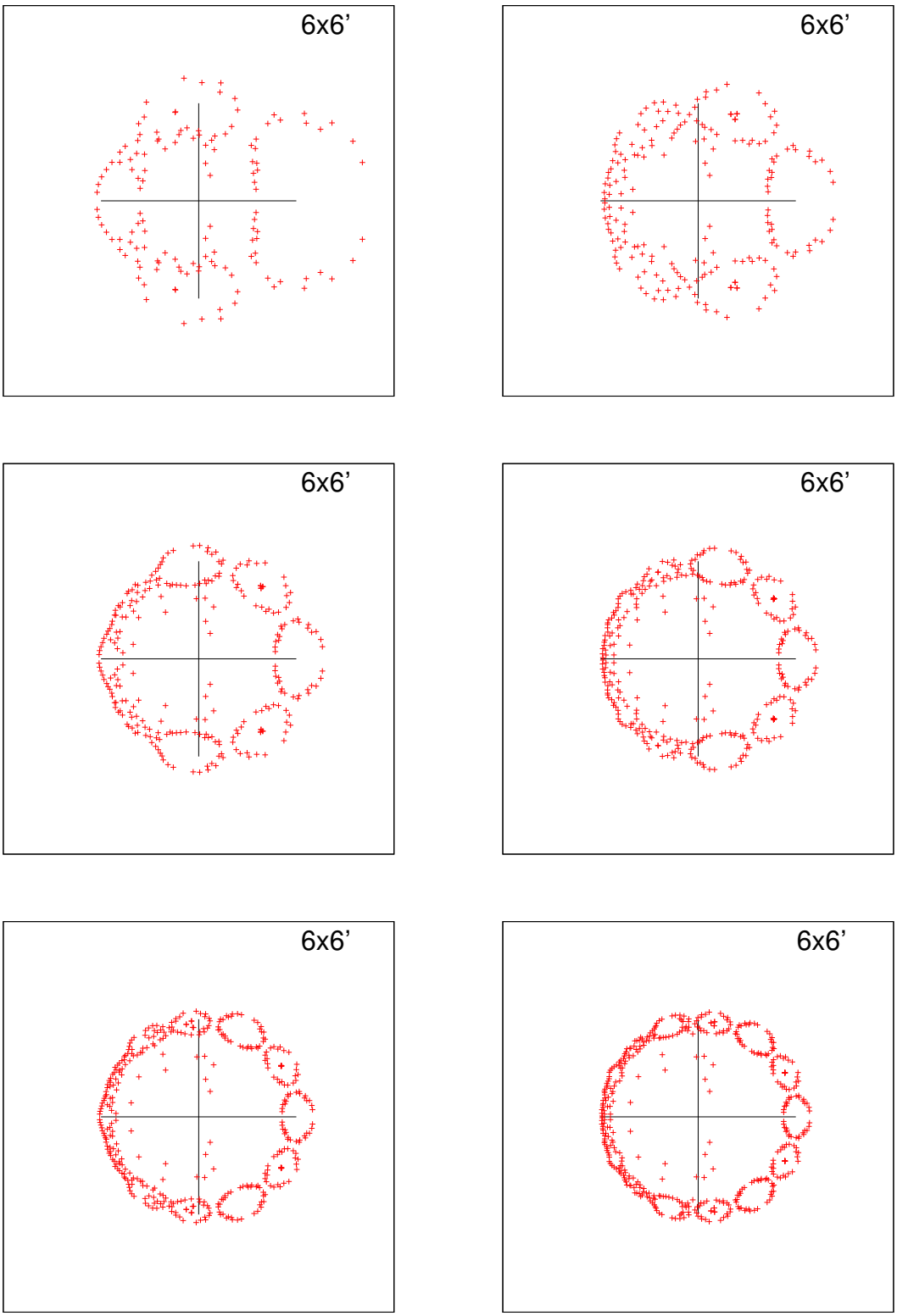

Figure 18: Zeros in $e^{-\beta}$ for the $\chi = (0, A, 0, A-1)$ 6-state model for $A = 2, 3, 4, 5, 6, 7$ with lattices size $6 \times 6'$. The scale is set by unit length of the positive real axis.

On lattices of fixed width. A summary of the basic analytical theory of zero distributions is given in [41, Ch.11]. In particular it is noted there (see also [40]) that Potts models on fixed-width strips are essentially integrable, and the limit curves of zeros are explained formally in terms of the underlying complex analysis. Specific examples are computed for example in [40]. This line of investigation has been revisited several times since. See for example [14]. While such approaches allow a superficial comparison of loci, a key point is that it is known that none of the finite-width models have a phase transition (they are better thought of as exotic 1D models). So allowing one direction of the lattice to grow much longer than the other is exactly the wrong thing to do for our purposes. Nonetheless, many of the results of Chang, Salas, Shrock et al are of considerable intrinsic beauty. The approach to 2D via *sequences* of fixed-width models is of course directly fruitful — see e.g. Blote *et al* [9]. This is one of the CFT aspects mentioned in the Introduction. For works looking at semi-infinite strip lattices see for example [7] and [40, 41], and cf. [14, 28, 46, 47].

Returning to Saleur [48], it is interesting to consider the unphysical dual point of the AF critical point. It is natural also to consider the 3-state Potts model on the triangular lattice, as done by Maillard–Martin: see for example [31, 42, 55]. These topics are outside the scope of the present paper.

Lee–Yang zeros (in the magnetic field as opposed to, as it were, fugacity) are another intrinsically interesting area of study (see e.g. [19] for references). However they have a significantly different flavour, both analytically and physically, to fugacity zeros.

On computation — transfer matrix realisations and algebra. There are many methods in principle for computing the Potts partition function (see e.g. [39–41]). We have benchmarked several of them and found (for the specific problem studied here) a direct transfer matrix approach to be effective. This paper is about results rather than computation, but for completeness we include here a set of references discussing various beautiful computational approaches. In its purest form this can be seen as a study of the representation theory of the Temperley–Lieb algebra [52] (or for higher dimensional Potts models the partition algebra [37]). From the 'spectral' point of view the TL algebra is completely understood, and the main Theorem is here [41, §7.3]. From the computational point of view the variants correspond in some cases to changing the representation (each one derived from an equivalent lattice model), and in some cases to changing the basis for the representation. For further references on the dichromatic polynomial approach and periodicity see for example [29, 30]; for RSOS models [45]; for the Fortuyn–Kastelyn approach [14]; for graph–theoretic methods [50]; and for the height-model approach [10, 12, 18, 46]. Note that, in practice, in the transfer matrix approach imposing periodic boundary directions in the 'time' direction reduced the size of lattice accessible to computation with given resources.

7 Acknowledgment

PM thanks EPSRC (grant EP/I038683/1), and SFZ thanks the International Islamic University Malaysia (RIGS17-051-0626) for partially supporting this manuscript preparation. The authors thank the University of Leeds. We thank our referees for several helpful comments.

References

[1] Abe, R. (1967). Logarithmic singularity of specific heat near the transition point in the Ising model. *Progress of Theoretical Physics*, 37(6):1070–1079.

[2] Baxter, R. J. (1970). Three-colorings of the square lattice: A hard squares model. *Journal of Mathematical Physics*, 11:3116.

[3] Baxter, R. J. (1973). Potts model at the critical temperature. *Journal of Physics C: Solid State Physics*, 6(23):L445.

[4] Baxter, R. J. (1982a). Critical antiferromagnetic square-lattice Potts model. *Proc. Roy. Soc. London*, 383:43.

[5] Baxter, R. J. (1982b). *Exactly Solved Models in Statistical Mechanics*. Academic Press Limited.

[6] Baxter, R. J. (1995). Solvable model in Statistical Mechanics, from Onsager onward. *Journal of Statistical Physics*, 78(1-2):7–16.

[7] Beraha, S., Kahane, J., and Weiss, N. (1975). Limits of zeroes of recursively defined polynomials. *Proceedings of the National Academy of Sciences of the United States of America*, 72:4209.

[8] Bhanot, G. and Sastry, S. (1990). Solving the Ising model exactly on a 5x5x4 lattice using the connection machine. *Journal of Statistical Physics*, 60:333–346.

[9] Blote, H. W. J., Cardy, J. L., and Nightingale, M. P. (1986). Conformal invariance, the central charge, and universal finite-size amplitudes at criticality. *Phys Rev Lett*, 56:742.

[10] Burton, J. K. and Henley, C. L. (1997). A constrained Potts antiferromagnet model with an interface representation. *Journal of Physics A: Mathematical and General*, 30(24):8385–8413.

[11] Candu, C. and Ikhlef, Y. (2013). Nonlinear integral equations for the sl(2, $\mathbb{R}$)/u(1) black hole sigma model. *Journal of Physics A: Mathematical and Theoretical*, 46(41):415401.

[12] Cardy, J., Jacobsen, J. L., and Sokal, A. D. (2001). Unusual corrections to scaling in the 3-state Potts antiferromagnet on a square lattice. *Journal of Statistical Physics*, 105:25–47.

[13] Cardy, J. L. (1996). *Scaling and Renormalization in Statistical Physics*. Cambridge.

[14] Chang, S. C., Salas, J., and Shrock, R. (2002). Exact Potts model partition functions for strips of the square lattice. *Journal of Statistical Physics*, 107:1207–1253.

[15] Chen, C.-N., Hu, C.-K., and Wu, F. (1996). Partition function zeros of the square lattice Potts model. *Physical review letters*, 76(2):169.

[16] Einhorn, M. B., Savit, R., and Rabinovici, E. (1980). A physical picture for the phase transitions in Z_n symmetric models. *Nuclear Physics B*, 170(1):16 – 31.

[17] Elitzur, S., Pearson, R. B., and Shigemitsu, J. (1979). Phase structure of discrete abelian spin and gauge systems. *Phys. Rev. D*, 19:3698–3714.

[18] Ferreira, S. J. and Sokal, A. D. (1999). Antiferromagnetic Potts models on the square lattice: A high-precision Monte Carlo study. *Journal of Statistical Physics*, 96.

[19] Fisher, M. E. (1965). The nature of critical points. In Britten, W. E., editor, *Lectures in Theoretical Physics*, volume 7c, pages 1–159. University of Colorado Press, Boulder.

[20] Flajolet, P. and Vardi, I. (1996). Zeta function expansions of classical constants. `http://algo.inria.fr/flajolet/Publications/landau.ps`.

[21] Hintermann, A., Kunz, H., and Wu, F. Y. (1978). Exact results for the Potts model in two dimensions. *Journal of Statistical Physics*, 19(6):623–632.

[22] Huang, K. (1987). *Statistical Mechanics*. John Wiley & Sons Ltd., second edition.

[23] Huse, D. A. (1984). Exact exponents for infinitely many new multicritical points. *Phys. Rev. B*, 30:3908–3915.

[24] Ikhlef, Y., Jacobsen, J., and Saleur, H. (2008). A staggered six-vertex model with non-compact continuum limit. *Nuclear Physics B*, 789:483–524.

[25] Ikhlef, Y., Jacobsen, J. L., and Saleur, H. (2009). A Temperley–Lieb quantum chain with two- and three-site interactions. *Journal of Physics A: Mathematical and Theoretical*, 42(29):292002.

[26] Ikhlef, Y., Jacobsen, J. L., and Saleur, H. (2010). The staggered vertex model and its applications. *Journal of Physics A: Mathematical and Theoretical*, 43:225201.

[27] Ikhlef, Y., Jacobsen, J. L., and Saleur, H. (2012). Integrable spin chain for the black hole sigma model. *Physical review letters*, 108:081601.

[28] Jacobsen, J. and Salas, J. (2000). Transfer matrices and partition-function zeros for antiferromagnetic Potts models II. extended results for square-lattice chromatic polynomial. *Journal of Statistical Physics*, 104.

[29] Jacobsen, J. L. (2014). High-precision percolation thresholds and Potts-model critical manifolds from graph polynomials. *Journal of Physics A: Mathematical and Theoretical*, 47:135001.

[30] Jacobsen, J. L., Richard, J., and Salas, J. (2006). Complex-temperature phase diagram of Potts and RSOS models. *Nuclear Physics B*, 743:153–206.

[31] Jacobsen, J. L., Salas, J., and Sokal, A. D. (2003). Transfer matrices and partition-function zeros for antiferromagnetic Potts models III. triangular-lattice chromatic polynomial. *Journal of Statistical Physics*, 112:921–1017.

[32] Jacobsen, J. L. and Saleur, H. (2006). The antiferromagnetic transition for the square-lattice Potts model. *Nuclear Physics B*, 743:207–248.

[33] Kaufman, B. (1949). Crystal Statistics. II. Partition function evaluated by spinor analysis. *Phys. Rev.*, 76:1232–1243.

[34] Kim, S.-Y. (2004). Density of the Fisher zeros for the three-state and four-state Potts models. *Physical review. E, Statistical, nonlinear, and soft matter physics*, 70:016110.

[35] Lieb, E. H. (1967a). Exact solution of the problem of the entropy of two-dimensional ice. *Physical Review Letters*, 18:692–694.

[36] Lieb, E. H. (1967b). Residual entropy of square ice. *Phys. Rev.*, 162:162–172.

[37] Martin, P. and Saleur, H. (1993). On an algebraic approach to higher-dimensional statistical mechanics. *Comm. Math. Phys.*, 158(1):155–190.

[38] Martin, P. P. (1983). Finite lattice Z(3) models in two and three dimensions. *Nuclear Physics B*, 225(4):497–504.

[39] Martin, P. P. (1985). Potts models and dichromatic polynomials. In Giacomo M. D′Ariano and Mario Rasetti, editors, *Integrable Systems in Statistical Mechanics*, pages 129–142. World Scientific.

[40] Martin, P. P. (1986). Analytic properties of the partition function for statistical mechanical models. *Journal of Physics A: Mathematical and General*, 19(16):3267–3277.

[41] Martin, P. P. (1991). *Potts Models and Related Problems in Statistical Mechanics*. World Scientific Pub Co Inc.

[42] Martin, P. P. (2000). Zeros of the partition function for the triangular lattice three-state Potts model II. `http://www1.maths.leeds.ac.uk/~ppmartin/ZEROS/pdf/q3tri2x.pdf`.

[43] Onsager, L. (1944). Crystal Statistics. I. A two-dimensional model with an order-disorder transition. *Phys. Rev.*, 65:117–149.

[44] Pearson, R. B. (1982). Partition function of the Ising model on the periodic 4x4x4 lattice. *Phys. Rev. B*, 26:6285–6290.

[45] Richard, J.-F. and Jacobsen, J. L. (2005). Relations between Potts and RSOS models on a torus. *Nuclear Physics B*, 731:335–351.

[46] Salas, J. and Sokal, A. D. (1998). The three-state square-lattice Potts antiferromagnet at zero temperature. *Journal of Statistical Physics*, 92:729–753.

[47] Salas, J. and Sokal, A. D. (2001). Transfer matrices and partition-function zeros for antiferromagnetic Potts models I, general theory and square-lattice chromatic polynomial. *Journal of Statistical Physics*, 104:609–699.

[48] Saleur, H. (1991). The antiferromagnetic Potts model in two dimensions: Berker-Kadanoff phase, antiferromagnetic transition, and the role of Beraha numbers. *Nuclear Physics B*, 360:219–263.

[49] Savit, R. (1980). Duality in field theory and statistical systems. *Rev. Mod. Phys.*, 52:453–487.

[50] Scullard, C. R. and Jacobsen, J. L. (2012). Transfer matrix computation of generalized critical polynomials in percolation. *Journal of Physics A: Mathematical and Theoretical*, 45:494004.

[51] Sloane, H J A (editor) (1964). The on-line encyclopedia of integer sequences. sequence at. `http://oeis.org/A092297`.

[52] Temperley, H. N. V. and Lieb, E. H. (1971). Relations between the 'percolation' and 'colouring' problem and other graph-theoretical problems associated with regular planar lattices: Some exact results for the 'percolation' problem. *Proceedings of the Royal Society of London. Series A, Mathematical and Physical Sciences*, 322(1549):251–280.

[53] Thompson, R. M. and Downs, R. T. (2001). Systematic generation of all nonequivalent closest-packed stacking sequences of length n using group theory. *Acta Crystallographica*, B57:766–771.

[54] Valani, Y. P. (2011). *On the Partition Function for the Three-dimensional Ising model*. PhD thesis, School of Engineering and Mathematical Sciences, City University, London, United Kingdom.

[55] Vernier, E., Jacobsen, J. L., and Salas, J. (2016). Q-colourings of the triangular lattice: exact exponents and conformal field theory. *Journal of Physics A: Mathematical and Theoretical*, 49(17):174004.

[56] von Gehlen, G. and Rittenberg, V. (1986). Operator content of the three-state Potts quantum chain. *Journal of Physics A: Mathematical and General*, 19(10):L625.

[57] Wannier, G. (1966). *Statistical Physics*. Dover Books on Physics. Dover Publications.

[58] Wu, F. Y. (1982). The Potts model. *Rev. Mod. Phys.*, 54:235–268.

[59] Yeomans, J. M. (1992). *Statistical Mechanics of Phase Transitions*. Oxford University Press.

[60] Zakaria, S. F. (2017). *Analytic Properties of Potts and Ising model Partition Functions and the Relationship between Analytic Properties and Phase Transitions in Equilibrium Statistical Mechanics*. PhD thesis, School of Mathematics, University of Leeds, United Kingdom. http://etheses.whiterose.ac.uk/16323/.